IET Image Processing

Research Article

IET Journals
The Institution of Engineering and Technology

End to end system for hazy image classification and reconstruction based on mean channel prior using deep learning network

ISSN 1751-9659
Received on 18th June 2020
Revised 15th December 2020
Accepted on 7th January 2021
doi: 10.1049/iet-ipr.2020.0923
www.ietdl.org

Sivaji Satrasupalli[1] ✉, Ebenezer Daniel[1], Sitaramanjaneya Reddy Guntur[1], Shaik Shehanaz[1]

[1]Vignan's Foundation for Science Technology and Research, Department of Electronics and Communications Engineering, Vadlamudi, Guntur, AP, 522213, India

✉ *E-mail: sivaji.ganesh1100@gmail.com*

Abstract: Outdoor images are having several applications including autonomous vehicles, geo-mapping, and surveillance. It is a common phenomenon that the images captured outdoor are prone to noise, which arises due to natural and manmade extreme atmospheric conditions such as haze, fog, and smog. Importantly in autonomous vehicle navigation, it is very important to recover the ground truth image to get the better decision by the system. Estimation of the transmission map and air-light is very crucial in recovering the ground truth image. In this study, the authors proposed a new method to estimate the transmission map based on a mean channel prior (MCP), which represents the depth map to estimate the transmission map. The authors proposed a deep neural network to identify the hazy image for the further dehazing process. In this study, the authors presented, two novel contributions, first an MCP-based image dehazing and second, a deep neural network-based identification of hazy images as a pre-processing block in the proposed end to end system. The proposed deep learning network using the TensorFlow platform provided validation accuracy of 93.4% for hazy image classification. Finally, the proposed MCP-based dehazing network showed better performance in terms of peak-signal-to-noise ratio, structural similarity index, and computational time than that of existing methods.

1 Introduction

Poor visibility is a challenging problem in recovering the ground truth. Recently, many researchers have contributed to solving this problem. Haze is essentially composed of aerosol, tiny suspended particles, and fog responsible for an increase in relative humidity in the air to reach saturation [1]. Hence haze and fog have the same origin and limits visibility. In many applications, it is required to automatically detect the hazy image and apply appropriate algorithms to recover the original radiance for the detection of objects for further processing like segmentation, object detections, and various vision applications [2]. As the concentration of haze is directly correlated to the depth of the object and having no information about depth poses a challenging task [3]. Kumar *et al*. [4] proposed colour uniformity principle for estimating the transmission map but airlight estimation is prone to error in different haze conditions. The work of Gao *et al*. [5] is based on the local linear fusion of gamma-corrected grey image and subtracted haze layer image, having a problem of generalisation to different images. Narasimhan and co-authors proposed a dehazing algorithm based on multiple images, taken under different degrees of polarisation. Though it produces impressive results, it is extremely inconvenient to take multiple images in real-time. In past, there is a remarkable improvement made in single image dehazing techniques by various researchers. Image enhancement techniques like contrast-limited adaptive histogram equalisation (CLAHE) and retinex methods were applied for haze removal. CLAHE was developed for medical images and has shown better performance but for hazy images, results are not visually competent [6]. Retinex theory shows better performance if the illumination is insufficient [7] but haze removal is completely different and depends on the depth of the object. Tan proposed a novel single image haze removal by enhancing the local contrast of the image based on Markov random fields, but it is having a problem of colour shifting [8]. Fattal proposed independent component analysis for haze removal, but the approach is time-consuming [9]. The minimum channel prior (MCP) based on the statistical conclusion that all the field images will be having at least one colour channel value low and very close to zero and the transmission map was estimated based on this prior but as the refinement of transmission map was done based on soft matting it was very time consuming [10].

There were various modifications introduced in the conventional DCP approach to improve the visibility of hazy images such as guided filter instead of soft matting for single-image dehazing [11]. Also, made various changes such as fusion of high-frequency components and near-infrared image [12], usage of surround filter [13] with DCP for dehazing and average saturation prior [14], respectively, for estimating the transmission map. Linear transformation techniques such as minimum filtering, fast mean filtering, and geometric and natural features of outdoor images [15] were used for transmission map and airlight estimation and little improvement was shown over the application. The methods such as colour attenuation prior [16] and boundary constraint prior [17] were used. Distinctive colours in an image form tight clusters in clear images [18], all the outdoor images can be represented with a finite number of colours and forms haze line, which were used for dehazing in literature. In past, many DCP-dependent techniques were introduced for image dehazing application, which includes scene prior using reference retrieval [19], saliency map [20], adaptive wiener filter, [21] and non-local total variation (NLTV) regularisation [22]. Recently, Sahu and Seal [23] presented a new method for estimating the transmission map for the sky and non-sky regions based on luminance stretching and DCP, respectively, and applied sigmoid fusion for the process.

Artificial intelligence methods such as deep learning and machine learning are effectively used in various imaging applications. Cai *et al.* [24] proposed a deep learning-based single image dehazing net called DehazeNet using a convolutional network, by applying bilateral rectified linear unit activation function for transmission map estimation. Santra *et al.* [25] proposed patch quality comparator based single image dehazing using deep learning approach. All the above-proposed methods have shown remarkable improvement but still, have scope for further improvement. To the best of our knowledge, our work is the

first one to introduce image dehazing based on the MCP. In addition to MCP dehazing, we introduced a deep learning-based approach for hazy and non-hazy images classification as a pre-processing unit. Based on the limitations of the existing methods in the literature, we proposed the following:

- Hazy image classifier for automatic detection of hazy images to avoid unnecessary pre-processing of clear images.
- Computationally efficient depth estimation based on MCP for removal of haze.

The article is organized as follows: Section 1 presents the introduction, Section 2 discusses the scattering model, Section 3 explains the proposed method, Section 4 discusses the comparison of results, Section 5 presents the subjective analysis, and finally, in Section 6 the conclusions are discussed.

2 Atmospheric scattering model

Atmospheric scattering model can be represented by the following equation [2]:

$$I(x, y) = J(x, y) \cdot t(x, y) + (1 - t(x, y))A \tag{1}$$

where (x,y) are the coordinates of the pixel, $I(x, y)$ is scene radiance, $J(x, y)$ is the ground truth of the image and $t(x, y)$ is the transmission map and A is the airlight. Transmission map depends on the distance of the object with reference to the camera [2].

$$t(x, y) = e^{-\beta d} \tag{2}$$

where β is the attenuation coefficient and d (x,y) represents the depth of the object in the image at (x,y) coordinates. From the above two equations, we can understand that as the depth of the object tends towards infinity, $t(x)$ tends to zero, and $I(x) = A$. If the object is in the foreground, depth will be relatively low and (1) becomes $J(x,y) = I(x,y)$. If two unknowns namely $d(x)$ and A can be calculated, then the original scene radiance can be recovered from the distorted image. After estimating the two key parameters namely transmission map and airlight, ground truth can be extracted based on the following (3) by reorganising the (1) minimum and maximum values of transmission map were limited to 0.1 and 0.9, respectively, to avoid colour shift of bright object and thick haze.

$$J(x) = \frac{I(x) - A}{\min\left\{\max\left\{e^{-\beta d(x)}, 0.1\right\}, 0.9\right\}} + A \tag{3}$$

3 Proposed method

Our method is based on the statistical observation that most of the pixels in outdoor images will have intensities <110 in the scale of 0–255 integer pixel values. The proposed method is broadly classified into two parts namely classification and reconstruction. Intelligence is to be added to make any system automatic. For this reason, we have implemented a classifier based on CNN architecture to classify whether the captured image has suffered from haze/fog. If the classifier output is close to zero then we can conclude that the input image is clear and can be used for further processing immediately. In this paper, the proposed classifier achieves 93.4% accuracy. If the classifier outputs a value close to one, then the captured image has suffered from noise like fog/haze. This classifier helps to skip the clean images and reduces the pressure on the processor and requires no human interference. The algorithm was designed to process the input image if the classifier score is >0.6.

Table 1 Proposed deep learning network architecture using CNN

Layer (type)	Output Shape	Param #
conv2d_l (Conv2D)	**(none, 148, 148, 32)**	896
max_pooling2d_l (Max Pooling2)	(none, 74, 74, 32)	0
conv2d_2 (Conv2D)	(none, 72, 72, 64)	18496
max_pooling2d_2 (MaxPooling2)	(none, 36, 36, 64)	0
conv2d_3 (Conv2D)	(none, 3,4 34, 128)	73856
max_pooling2d_3 (MaxPooling2)	(none, 17, 17, 128)	0
conv2d_4 (Conv2D)	(none, 15, 15, 128)	147584
max_pooling2d_4 (Ma xPooling2)	(none, 7, 7, 128)	0
flatten_l (Flatten)	(none, 6272)	0
dropout_l (Dropout)	(none, 6272)	0
dense_l (Dense)	(none, 512)	3211776
dense_2 (Dense)	(none, 1)	513

Total params: 3,453,121; trainable params: 3,453,121; non-trainable params: 0

After classifier, depth map was estimated based on MCP, it is an average of the three channels namely red, green, and blue. The mean value is linearly correlated to the concentration of the haze and hence represents the depth map. Transmission map was estimated based on (5) and guided filter [9] was applied to remove any artefacts in the image. Finally, the dehazed output was restored based on (3). Hereafter the proposed method is organised as follows. Section 3.1 explains the classifier, Section 3.2 discusses the histogram relation of the haze and clear image, Section 3.3 is about the estimation of transmission map based on MCP, Section 3.4 is airlight estimation, and Section 3.5 deals with the scene radiance recovery.

3.1 Deep learning-based hazy image classifier

Our proposed deep learning network is inspired by ImageNet [26], we introduced a neural network to classify the Hazy image. A neural network generally consists of three layers namely the input layer, hidden layer, and output layer. The input layer will accept the hazy image, hidden layer, and output layer will act as non-linear functions to calculate the classifier score. Each hidden layer includes a convolution, max-pooling, and rectifier linear unit (ReLu) as the activation function. Convolution layer will calculate the features of the image progressively. Max-pooling layer is a down-sampling operation, which reduces the size of the image by taking maximum value in a 2×2 matrix. ReLu activation function is $\max(0,x)$ removes any negative values. Flatten layer converts any array into a single column vector and dropout layer randomly removes 50% of the weights to avoid overfitting problem. If overfitting happens, then the classifier produces better training accuracy but cannot generalise on unseen data and hence will not be useful for any practical applications. So dropout layer was added to improve the generalisation on unseen data. In densely connected layers all inputs are connected to all outputs by weights and useful in labelling the image class as hazy or clear. The output layer used softmax as activation function and produces an output value always within the range of 0 and 1. Table 1 shows the proposed architecture, which consists of four hidden layers and an output layer. Each hidden layer consists of convolution filters, max-pooling layers, and ReLus. The layers were densely connected, the fully connected layer consists of flattened layer, dense layer, and dropout layers. After defining the architecture, the performance is completely depending on the volume and variety of the data set. The data set was carefully designed by taking 2000 images from various resources like NYU Depth data set [27], RESIDE data set [28], Foggy Road Image Database (FRIDA) [29], and Google images. Data set is divided into training and validation data with 70:30 ratios. The architecture was trained on these images with batch size 100 images and epochs 50 on Keras platform and got validation accuracy of 93.4%.

3.2 Mean channel prior

In this work, we proposed a simple prior for reconstructing the hazy images based on MCP. Based on the extensive study using NYU Depth data set and RESIDE data set, it was observed that the mean value of three channels linearly increases with the increase in haze concentration. After comparing the histograms of mean values of ground truth and hazy image, it was statistically concluded that mean channel value increases with the increase in haze concentration, i.e. as depth increases. Fig. 1 shows that the mean

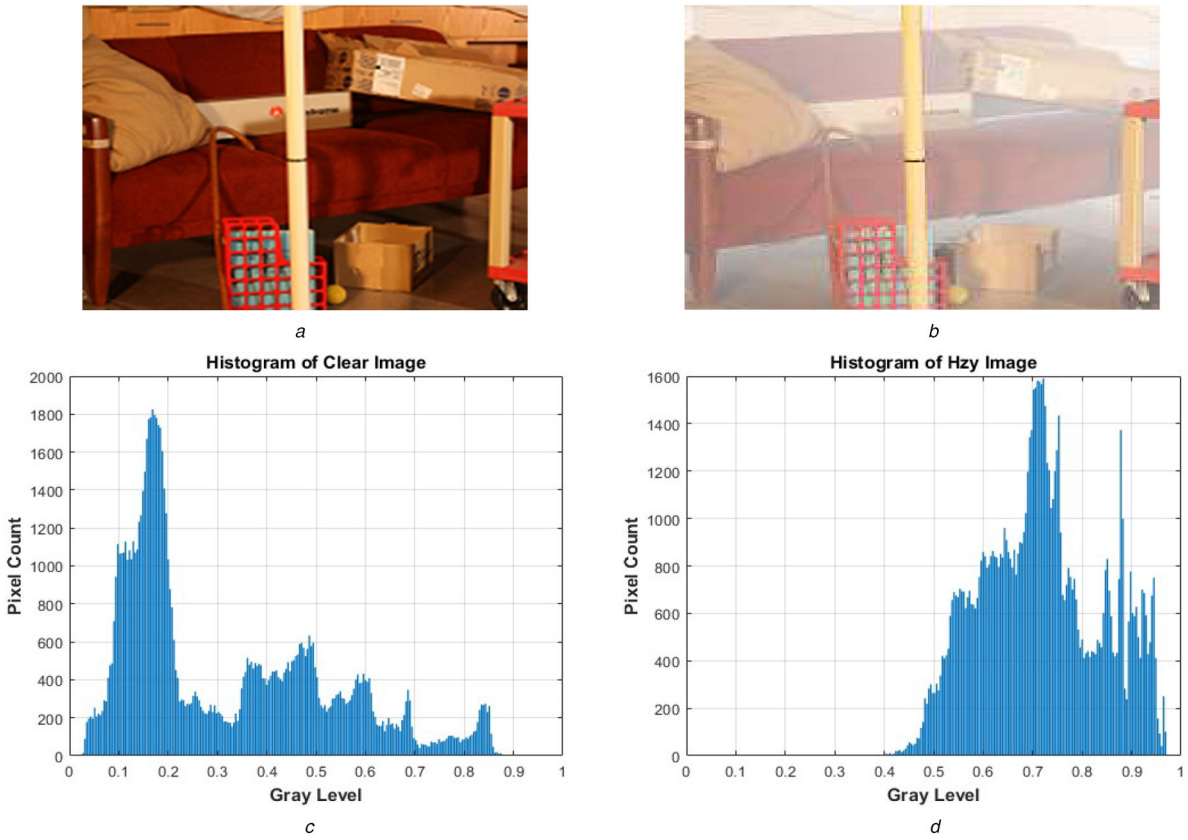

Fig. 1 *Histogram comparison of clear and hazy image.*
(a) Clear image, ***(b)*** Hazy image, ***(c)*** Histogram of (a), ***(d)*** Histogram of (b)

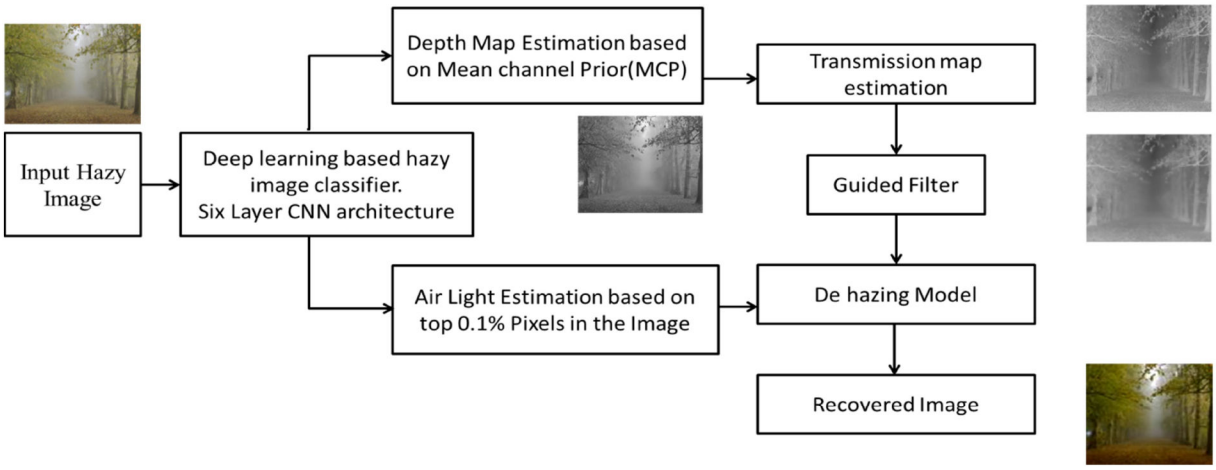

Fig. 2 *Proposed block diagram*

pixel values distributed in the entire scale and 75% pixel values are <0.6 but as haze concentration increases mean pixel values are concentrating at a relatively high value.

Mean channel of the hazy image can be calculated as follows:

$$\mathrm{Mc} = \left(\underset{c \in \mathrm{R,G,B}}{\mathrm{mean}} I^{C}(x, y) \right) \tag{4}$$

where I is the input hazy image, x is the index of the image and Mc is the mean channel which represents the concentration of haze and can be approximated as a depth map. Based on the atmospheric scattering model transmission map can be calculated with the following (5). Fig. 2 shows the intermediate results after applying the MCP in the atmospheric scattering model and Fig. 3*c* shows an example of MCP.

$$t(x, y) = e^{-\beta(\mathrm{Mc})} \tag{5}$$

where Mc is the depth map estimated from MCP and β is the atmospheric attenuation factor and is wavelength sensitive and hence it is different for three colour channels. Its impact was minimal as per the previous paper and in this paper also it is assumed to be the same.

Fast guided filter [34] was applied on the estimated transmission map $t(x,y)$ to smoothen without affecting the edges present in the original image. $G(x)$ is the output of the fast guided filter can be calculated as

$$G(x) = \overline{a_i} J(x) + \overline{b_i}, \forall_x \in \omega_i \tag{6}$$

where $J(x)$ is the guidance image, x is the index of the pixel, and i is the index of the local window ω with radius k. $\overline{a_i}$ and $\overline{b_i}$ are averages of a and b in the window ω. Given the transmission map $t(x)$ as filtering input and minimising the error between $G(x)$ and $t(x)$ gives

$$a_i = \frac{\frac{1}{|\omega|}\sum_{X \in \omega_i} J(x)t(x) - \mu_i \bar{t_i}}{\sigma_i^2 + \in} \tag{7}$$

$$b_i = \bar{t_i} - a_i \mu_i \tag{8}$$

where μ_i and σ_i are mean and variance of $J(x)$ in the window ω and ϵ is used for controlling the smoothness.

3.3 Atmospheric light calculation

Another important factor in solving the haze model (3) is the estimation of airlight (A). As per the haze model, brightness significantly increases as haze concentration increases, the highest value of the input image as atmospheric light A considered in [4]. However, sometimes images might include white objects brighter than the actual A, which potentially misleads the estimation. So in this paper, airlight was estimated based on the average of top 0.1% pixels of the dark channel [10]. The dark channel can be calculated as

$$J_{\text{dark}}(X) = \min_{C \in \text{r, g, b}} J^C(X) \tag{9}$$

$J_{\text{dark}}(x)$ is the minimum channel in the given input $J(x)$. Airlight can be calculated based on (9) as follows:

$$A = \frac{\sum_{i=0}^{n} J_{\text{dark}}(i)}{n} \tag{10}$$

where n is the 0.1% equivalent number of pixels in $J_{\text{dark}}(x)$ in ascending order so that only brightest pixels will be considered.

3.4 Scene radiance recovery

After calculating the transmission map and airlight, we have reconstructed the scene radiance from (1). The final scene radiance can be recovered by (11), by reorganising the (1), ground truth J(x,y) can be written as

$$J(x, y) = \frac{I(x, y) - A}{t(x, y)} + A \tag{11}$$

ground truth can be retrieved by substituting the (6) and (10) in (11). To avoid colour shift of bright objects transmission map was limited in the boundary of (0.1,0.9), which results in the following equation:

$$J(x, y) = \frac{I(x, y) - A}{\min\{\max\{G(x), 0.1\}, 0.9\}} + A \tag{12}$$

4 Experiment results and discussion

Next, we compare the performance of the proposed algorithm with the three state-of-the-art methods on both synthetic images and real-world images.

4.1 Data collection

For hazy image classification, it is required to have both hazy and haze-free images. We have manually selected 2000 hazy and haze-free images from NYU Depth data set, Google, FRIDA [29] and RESIDE Data set. We have set the classification score as 0.6 for identifying the hazy image. Some of the hazy images were shown in Figs. 4*a–d* was taken from Middlebury and IHAZE data set.

4.2 Hazy image classification

The proposed CNN architecture was trained on the manually tailored data set. We have set the parameter of architecture as batch size 100, the number of epochs 50 and 50% dropout. Dropout layer [31] is an effective method for regularisation and proved to improve validation accuracy. The validation accuracy of the classifier on unseen data was achieved as 93.4%.

The hazy classifier was trained on Keras library in Google Colaboratory. Fig. 5 shows the training and validation accuracies versus the number of epochs.

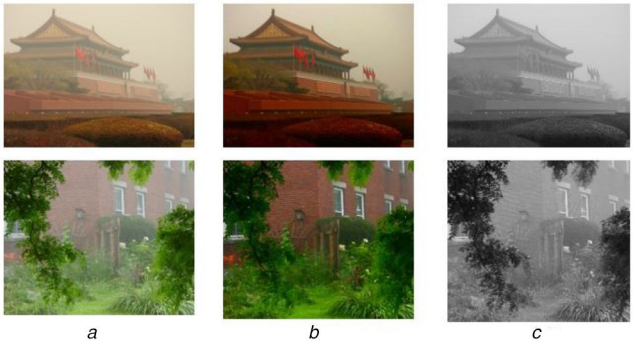

Fig. 3 *Overview of the proposed method*
(a) Input distorted image, ***(b)*** Restored image, ***(c)*** Mean channel

4.3 Comparisons on synthetic images

The proposed algorithm was quantitatively verified and compared with the three state-of-the-art methods on Middlebury D-haze data set [32] and IHAZE data set [33]. Fig. 4 shows the sample of both Middlebury hazy images IHAZE images, Figs. 6–9 shows the results of Wang *et al.*'s method [3], Cai *et al.*'s method [24], and Zhu *et al.*'s method [16], respectively. Dehazing results of Wang *et al.*'s method [3] suffer from a colour shift and artefacts at edges, Cai *et al.*'s method [24] and Zhu *et al.*'s method [16] is still having haze. Although the proposed method also has traces of haze but fairly good with respect to colour shift and artefacts. All these four methods were compared quantitatively on Middlebury D-haze data set. We have taken the structural similarity index (SSIM) and the peak-signal-to-noise ratio (PSNR) as performance metrics [30]. Table 2 shows the comparison of SSIM and PSNR, the last row shows average values for 18 images. The proposed method was good with classroom1 and flower images and fairly good with reaming as the proposed method is very simple and proved to be robust. The proposed method also validated on IHAZE data set. Tables 3 and 4 show the comparisons of the SSIM and PSNR with IHAZE data set. The results produced by the proposed method are on par with Cai's method and outperforms the remaining methods.

The PSNR and structural SSIM was evaluated as follows:

$$\text{PSNR}(f, g) = 10\log\left(\frac{255^2}{\text{MSE}(f, g)}\right) \tag{13}$$

$$\text{MSE}(f, g) = \frac{1}{\text{MN}}\sum_{i=1}^{M}\sum_{j=1}^{N}\left(f_{ij} - g_{ij}\right)^2 \tag{14}$$

$$\text{SSIM}(f, g) = \frac{(2\mu_f\mu_g + C_1)(2\sigma_{fg} + C_2)}{(\mu_f^2 + \mu_g^2 + C_1)(\sigma_f^2 + \sigma_g^2 + C_2)} \tag{15}$$

where f and g are the reference and restored images, $\mu_f, \mu_g, \sigma_f, \sigma_g, \sigma_{fg}$ are local means, standard deviations, and cross-correlations.

4.4 Execution time

The efficiency of the proposed method was compared with state-of-the-art methods. We have computed the computation complexity of different images with different sizes. All methods have been executed in MATLAB 2019b with the same computer (LENOVO Laptop with processor i5-3210M at 2.50 GHz and 8.0 GB RAM). Table 5 shows the comparison with the state-of-the-art methods and the proposed method outperforms all the methods for small images in the order of 200 × 200 (computational time excluding the

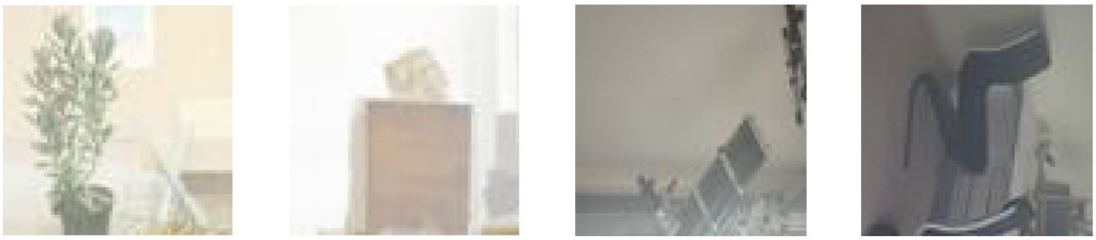

a *b* *c* *d*

Fig. 4 *Sample hazy images*
(a), ***(b)*** From Middlebury, ***(c)***, ***(d)*** From IHAZE data set

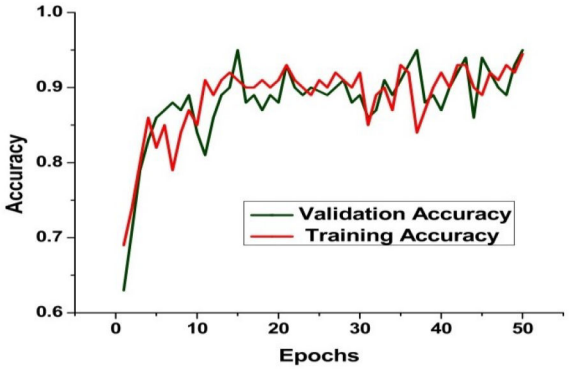

Fig. 5 *Training and validation accuracy*

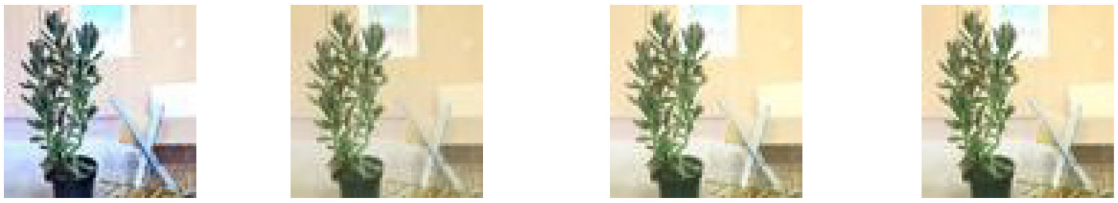

a *b* *c* *d*

Fig. 6 *Results on Middlebury D-Haze data set on sword 1*
(a) Wang *et al.*'s method [3], ***(b)*** Cai *et al.*'s method [24], ***(c)*** Zhu *et al.*'s method [16], ***(d)*** Proposed

a *b* *c* *d*

Fig. 7 *Results on Middlebury D-Haze data set on the storage*
(a) Wang *et al.*'s method [3], ***(b)*** Cai *et al.*'s method [24], ***(c)*** Zhu *et al.*'s method [16], ***(d)*** Proposed

a *b* *c* *d*

Fig. 8 *Results on music instruments image from IHaze data set*
(a) Wang *et al.*'s method [3], ***(b)*** Cai *et al.*'s method [24], ***(c)*** Zhu *et al.*'s method [16], ***(d)*** Proposed

classifier) and performs well for large images except Wang's method [3].

We have executed the 1 Mpixel image four times and noted the average time taken for each block. The total time taken for the reconstruction of the hazy image is given as

$$T(\text{ms}) = T_{\text{MC}-} + T_{\text{FG}+}T_{\text{AL}} + T_{\text{Recovery}} \tag{16}$$

where T_{MC}, T_{FG}, T_{AL}, T_{Recovery} are the time taken for mean channel calculation, applying the fast-guided filter, airlight estimation, and for scene radiance recovery in milliseconds.

Typical values of T_{MC}, T_{FG}, T_{AL}, $T_{Recovery}$ for 1 Mpixel are 33, 1300, 31, and 42 ms, respectively. The total time taken for 1000 × 1000 image is 1.57 s and for 200 × 200 image is 0.14 s. It was observed that computational time increases exponentially for image

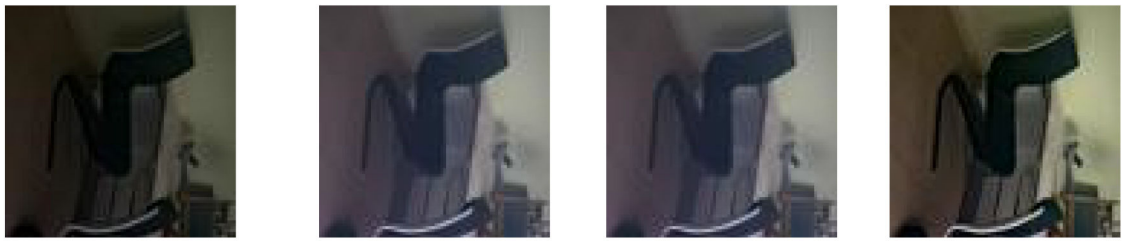

a *b* *c* *d*

Fig. 9 *Results on chair image from IHaze data set*
(a) Wang *et al*.'s method [3], ***(b)*** Cai *et al*.'s method [24], ***(c)*** Zhu *et al*.'s method [16], ***(d)*** Proposed

Table 2 Comparison of SSIM and PSNR with Middlebury D-hazy data set

	Wang *et al*.'s method [3]		Cai *et al*.'s method [24]		Zhu *et al*.'s method [16]		Proposed	
	SSIM	PSNR	SSIM	PSNR	SSIM	PSNR	SSIM	PSNR
vintage	0.84	17	0.865	16.72	0.94	18.52	0.94	18.54
umbrella	0.69	14.81	0.85	15.4	0.85	15.6	0.86	15.5
sword 2	0.77	14.11	0.81	18.5	0.68	12.9	0.7	12.6
sword 1	0.27	12.41	0.85	15.07	0.86	15.36	0.86	14.9
storage	0.63	15.14	0.78	15	0.79	11.9	0.74	11.29
sticks	0.86	18.8	0.82	16.8	0.94	20.6	0.95	20.5
shelves	0.88	19.97	0.9	19.79	0.88	18.67	0.89	18.9
recycle	0.81	13.8	0.9	17.12	0.92	18.97	0.9	17.82
play table	0.78	16.9	0.87	16.14	0.83	16.54	0.8	16.3
playroom	0.83	16.7	0.8	14.5	0.83	15.94	0.78	15.1
adirondack	0.8	13.63	0.85	15.4	0.84	14.6	0.87	14.9
backpack	0.84	15.82	0.84	16.2	0.81	15.4	0.84	15.8
bicycle 1	0.8	15.4	0.94	20.9	0.9	18.3	0.96	20.5
cable	0.58	6.6	0.64	8.13	0.64	8	0.67	8.83
classroom 1	0.85	17.2	0.72	10.9	0.79	12.92	0.8	13.88
couch	0.66	14.19	0.68	11.5	0.72	12.64	0.78	13.4
flowers	0.8	13.44	0.74	10.5	0.74	10.5	0.75	12.62
mask	0.73	15.29	0.8	15.4	0.76	14.66	0.74	14.2
Average	0.72	14.25	0.79	14.72	0.78	14.45	0.79	14.59

Table 3 SSIM comparison on IHAZE data set

Number	Wang *et al*.'s method [3]	Cai *et al*.'s method [24]	Zhu *et al*.'s method [16]	Proposed
1	0.31	0.67	0.149	0.59
2	0.36	0.73	0.2	0.61
3	0.44	0.44	0.04	0.47
4	0.27	0.32	0.03	0.31
5	0.6	0.62	0.09	0.59

Table 4 PSNR comparison on IHAZE data set

Number	Wang *et al*.'s method [3]	Cai *et al*.'s method [24]	Zhu *et al*.'s method [16]	Proposed
1	9.8	13.8	6.06	10.3
2	12.67	15.55	8.18	14.93
3	11.46	15.54	8.89	14.42
4	8.45	9.18	7.78	9.09
5	11.26	16.81	8.66	15.6

Table 5 Computational time (seconds) analysis obtained on Middlebury d-hazy data set

Size of the image	Wang *et al*.'s method [3]	Cai *et al*.'s method [24]	Zhu *et al*.'s method [16]	Proposed
200 × 200	0.34	0.59	0.97	0.14
400 × 400	0.4	1.9	12.9	0.45
1000 × 1000	1.04	9.8	11.9	1.57
2864 × 2008	3.4	65.24	20.6	3.46
2356 × 1996	2.77	54	7.8	2.8

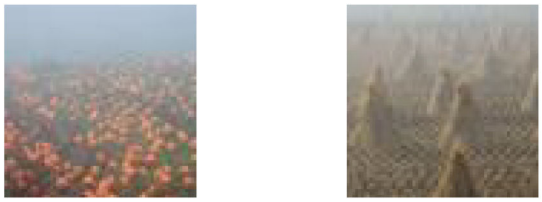

Fig. 10 *Sample real-world hazy images*

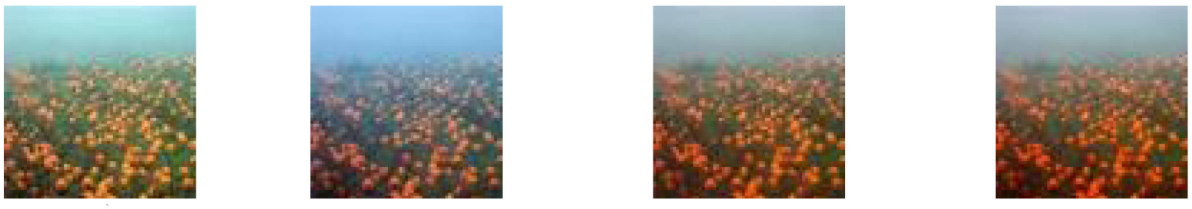

Fig. 11 *Results on real world pumpkin field image*
(a) Wang's method [11], ***(b)*** Cai's method [19], ***(c)*** Zhu *et al.*'s method [12], ***(d)*** Proposed

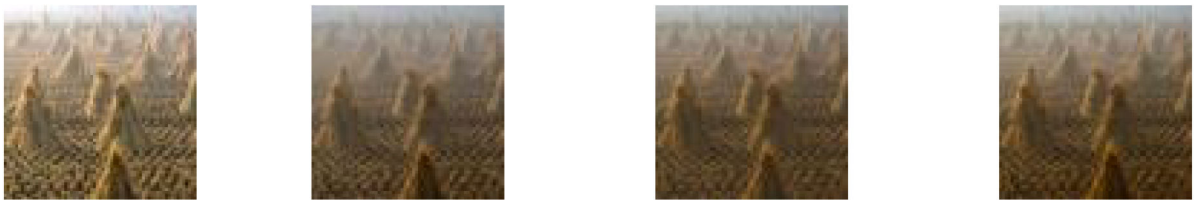

Fig. 12 *Results on real world cone image*
(a) Wang's method [11], ***(b)*** Cai's method [19], ***(c)*** Zhu *et al.*'s method [12], ***(d)*** Proposed

size beyond 1 Mpixel. The execution time of the proposed approach was relatively less due to its simplicity of mean value calculation and fast-guided filter. Cai *et al.*'s method [24] execution time substantially increases as image size increases due to its very complex trained model. Zhu *et al.*'s method [16] and Wang *et al.*'s method [3] are simple but their transmission map refinement algorithms were complex

5 Subjective analysis

Fig. 10 shows the sample real-world hazy images, Figs. 11 and 12 show the comparison of Wang *et al.*'s [3], Cai *et al.*'s [24], Zhu *et al.*'s methods [16] and the proposed method on real-world images. It can be noticed that the proposed method maintains the true colour of the image. Most of the outdoor images have colourful objects and their primary colour channel average was relatively low. In total, 80% of the pixels have values <0.6 (without sky region). It is found that the pixels that belong to the haze affected region are relatively high. The proposed method is not based on patch-wise processing but based on pixel-wise processing. Our proposed MCP-based technique showed better results compared with state-of-the-art methods with quantitative and qualitative analysis.

6 Conclusion

In this paper, we presented a deep neural network for classifying the hazy image for automatic detection of a hazy image, implemented, and got 93.4% validation accuracy over 50 epochs. Also, we introduced an MCP for image dehazing. Our MCP approach reduced the computational time without compromising at other performance metrics. Our technique provided better results in terms of PSNR and SSIM. Limitations of our study were also noted. We used 2000 image data sets for classification in the future we can improve the classification accuracy by adding more training data. However, the proposed method showed a colour shift at sky regions and colour saturation on IHAZE data set. The results have shown compromised performance on indoor hazy images and our future research is focused on segmentation and object identification in hazy images.

7 References

[1] Narasimhan, S.G., Nayar, S.K.: 'Vision and the atmosphere', *Int. J. Comput. Vis.*, 2002, **48**, (3), pp. 233–254

[2] Guo, L., Song, J., Li, X.R., *et al.*: 'Haze image classification method based on alexnet network transfer model', *In J. Phys.: Conf. Ser.*, 2019, **1176**, (3), pp. 1–7

[3] Wang, W., Yuan, X., Wu, X., *et al.*: 'Fast image dehazing method based on linear transformation', *IEEE Trans. Multimed.*, 2017, **19**, (6), pp. 1142–1155

[4] Kumar, H., Gupta, S., Venkatesh, K.S.: 'Realtime dehazing using colour uniformity principle', *IET Image Process.*, 2019, **13**, (11), pp. 1931–1939

[5] Gao, Y., Chen, H., Li, H., *et al.*: 'Single image dehazing using local linear fusion', *IET Image Process.*, 2017, **12**, (5), pp. 637–643

[6] Reza, A.M.: 'Realization of the contrast limited adaptive histogram equalization (CLAHE) for real-time image enhancement', *J. of VLSI Signal Process. Syst. For Signal, Image And Video Technol.*, 2004, **38**, (1), pp. 35–44

[7] Zhao, Y., Liu, Y., Song, K., *et al.*: 'A retinex theory based point sampling method'. Int. Conf. of Soft Computing and Pattern Recognition (SoCPaR), Hyderabad, India, 2011, pp. 330–335

[8] Tan, R.T.: 'Visibility in bad weather from a single image', IEEE Conf. on Computer Vision and Pattern Recognition., Anchorage, AK, USA, 2008, pp. 1–8

[9] Fattal, R.: 'Single image dehazing', *ACM Trans. Graph.*, 2008, **27**, (3), pp. 1–9

[10] He, K., Sun, J., Tang, X.: 'Single image haze removal using dark channel prior', *IEEE Trans. Pattern Anal. Mach. Intell.*, 2010, **33**, (12), pp. 2341–2353

[11] He, K., Sun, J., Tang, X.: 'Guided image filtering'. European Conf. On Computer Vision, Heraklion, Crete, Greece, 2010, pp. 1–14

[12] Jang, D.W., Park, R.H.: 'Colour image dehazing using near-infrared fusion', *IET Image Process.*, 2017, **11**, (8), pp. 587–594

[13] Nair, D., Sankaran, P.: 'Color image dehazing using surround filter and dark channel prior', *J. Vis. Commun. Image Represent.*, 2018, **1**, (50), pp. 9–15

[14] Gu, Z., Ju, M., Zhang, D.: 'A single image dehazing method using average saturation prior', *Math. Probl. Eng.*., 2017, **2017**, pp. 1–17

[15] He, R., Wang, Z., Fan, Y., *et al.*: 'Combined constraint for single image dehazing', *Electron. Lett.*, 2015, **51**, (22), pp. 1776–1778

[16] Zhu, Q., Mai, J., Shao, L.: 'A fast single image haze removal algorithm using color attenuation prior', *IEEE Trans. Image Process.*, 2015, **24**, (11), pp. 3522–3533

[17] Meng, G., Wang, Y., Duan, J., *et al.*: 'Efficient image dehazing with boundary constraint and contextual regularization'. Proc. IEEE Int. Conf. on Computer Vision., 2013, pp. 617–624

[18] Berman, D., Avidan, S.: 'Non-local image dehazing'. Proc. of the IEEE Conf. On Computer Vision And Pattern Recognition, Las Vegas, NV, USA, 2016, pp. 1674–1682
[19] Yuan, F., Huang, H.: 'Image haze removal via reference retrieval and scene prior', *IEEE Trans. Image Process.*, 2018, **27**, (9), pp. 4395–4409
[20] Zhang, L., Wang, S., Wang, X.: 'Saliency-based dark channel prior model for single image haze removal', *IET Image Process.*, 2018, **12**, (6), pp. 1049–1055
[21] Gibson, K.B., Nguyen, T.Q.: 'Fast single image fog removal using the adaptive Wiener filter'. IEEE Int. Conf. on Image Processing, Melbourne, Australia, 2013, pp. 714–718
[22] Liu, Q., Gao, X., He, L.*, et al.*: 'Single image dehazing with depth-aware non-local total variation regularization', *IEEE Trans. Image Process.*, 2018, **27**, (10), pp. 5178–5191
[23] Sahu, G., Seal, A.: 'Image dehazing based on luminance stretching'. Int. Conf. on Information Technology (ICIT), Bhubaneswar, India, 2019, pp. 388–393
[24] Cai, B., Xu, X., Jia, K.*, et al.*: 'Dehazenet: an end-to-end system for single image haze removal', *IEEE Trans. Image Process.*, 2016, **25**, (11), pp. 5187–5198
[25] Santra, S., Mondal, R., Chanda, B.: 'Learning a patch quality comparator for single image dehazing', *IEEE Trans. Image Process.*, 2018, **27**, (9), pp. 4598–4607
[26] Deng, J., Dong, W., Socher, R*, et al.*: 'Imagenet: A large-scale hierarchical image database', IEEE Conf. On Computer Vision and Pattern Recognition, Miami, FL, USA, 2009, pp. 248–255
[27] Silberman, N., Hoiem, D., Kohli, P.*, et al.*: 'Indoor segmentation and support inference from rgbd images'. European Conf. on Computer Vision, Firenze, Italy, 2012, pp. 746–760
[28] Li, B., Ren, W., Fu, D.*, et al.*: 'Reside: A benchmark for single image dehazing', arXiv preprint, 2017
[29] Tarel, J.P., Hautiere, N., Cord, A.*, et al.*: 'Improved visibility of road scene images under heterogeneous fog'. IEEE Intelligent Vehicles Symp., La Jolla, CA, USA, 2010, pp. 478–485
[30] Hore, A., Ziou, D.: 'Image quality metrics: PSNR vs. SSIM', Int. Conf. on Pattern Recognition, Istanbul, Turkey, 2010, pp. 2366–2369
[31] Srivastava, N., Hinton, G., Krizhevsky, A*, et al.*: 'Dropout: a simple way to prevent neural networks from overfitting', *J. Mach. Learn. Res.*, 2014, **15**, (1), pp. 1929–1958
[32] Ancuti, C., Ancuti, C.O., DeVleeschouwer, C.: 'D-hazy: A dataset to evaluate quantitatively dehazing algorithms', IEEE Int. Conf. on Image Processing (ICIP), Phoenix, AZ, USA, 2016, pp. 2226–2230
[33] Ancuti, C.O.., Ancuti, C., Timofte, R*, et al.*: 'I-HAZE: A dehazing benchmark with real hazy and haze-free indoor images', arXiv, 2018
[34] He, K., Sun, J.: 'Fast guided filter', arXiv preprint arXiv:1505.00996, 2015